Lawrence Berkeley National Laboratory

Title
Reactive Spreading of a Lead-Free Solder on Alumina

Permalink
https://escholarship.org/uc/item/3kp1t541

Authors
Gremillard, L.
Saiz, E.
Radmilovic, V.R.
et al.

Publication Date
2008-06-04

Peer reviewed

Reactive spreading of a lead-free solder on alumina

Laurent Gremillard[+#], Eduardo Saiz[+], Velimir R. Radmilovic[*], Antoni P. Tomsia[+]

[+]Materials Sciences Division, Lawrence Berkeley National Laboratory (MSD-LBNL), Berkeley, CA 94720, USA.

[*]National Center for Electron Microscopy, Lawrence Berkeley National Laboratory (NCEM-LBNL), Berkeley, CA 94720, USA.

[#] Materials Science Department, UMR CNRS 5510, National Institute of Applied Science (GEMPPM-INSA), 69621 Villeurbanne, France

Abstract

The wetting of Sn3Ag-based alloys on Al_2O_3 has been studied using the sessile-drop configuration. Small additions of Ti decrease the contact angle of Sn3Ag alloys on alumina from 115 to 23 degrees. Adsorption of Ti-species at the solid-liquid interface prior to reaction is the driving force for the observed decrease in contact angle, and the spreading kinetics is controlled by the kinetics of Ti dissolution into the molten alloy. The addition of Ti increases the transport rates at the solid-liquid interface, resulting in the formation of triple-line ridges that pin the liquid front and promote a wide variability in the final contact angles.

Introduction

New low-temperature brazing alloys are required in many applications to integrate components that decompose or degrade above threshold temperatures. Traditionally, a key component in the design of brazing alloys for ceramic joining is the addition of reactive elements such as Ti, Cr, Zr, etc., in order to enhance spreading. The improved wetting resulting from the addition of reactive elements is usually associated with the formation of new compounds at the solid-liquid interface. However, it is unproven whether compound formation is actually necessary for enhanced wetting, or mechanistically, how the potential for compound formation translates into the capillary forces that specifically drive spreading of the fluid. Recently, an alternative reactive wetting mechanism that focuses on the adsorption

of the reactive element at the solid-liquid interface before the nucleation of the reaction phase has been proposed as a critical step to reduce interfacial energy and drive spreading.[1]

Tin-silver-based alloys have emerged as a lead-free alternative to the traditional solders used in the microelectronics industry.[2–3] Sn-Ag-Ti alloys are also of theoretical interest. It has been observed that the wetting of Sn-based alloys on ceramics can be greatly enhanced by the addition of titanium, but in our work, no continuous reaction products could be detected at the metal–ceramic interface as is commonly observed in other systems.[1] These observations indicate that spreading to low contact angles can be driven by adsorption at the interface either without a reaction phase, or before one is formed. *In situ* neutron reflectometry studies of Sn-Ti/alumina interfaces have shown segregation of titanium at the ceramic-metal interface without formation of reaction products at the experimental temperature.[4] Derby et al.[4] have shown that interfacial oxides of Ti appear at the Ag-Cu-Ti/sapphire interface only after solidification.

The present work focuses on the study of the wetting behavior of Sn-Ag-Ti alloys on sapphire. The spreading of molten metals at different temperatures has been analyzed, and the interfacial transport phenomena are investigated via grain boundary grooving experiments. Evidence for an adsorption-driven spreading is presented.

Experimental

The wetting of Sn3Ag (3 wt% – 3.2 mol% Ag) and Sn3Ag1Ti alloys (1 wt% – 2.3 mol% Ti) on Al_2O_3 was studied using the sessile-drop configuration. The starting alloys had a typical tin-silver eutectic microstructure, with long Ag_3Sn platelets (ε phase) immersed in a tin matrix. In the titanium-containing alloys, Sn_5Ti_6 platelets ($\sim 15\times35$ μm) were dispersed throughout the metal.

Sessile drop experiments were conducted under vacuum (pressure ranging from 0.1 to 1 mPa) at temperatures ranging between 600 and 1000°C. A metal piece was placed on a flat sapphire or polycrystalline alumina substrate (grain size ~16 μm measured by the linear intercept method, prepared from a 99.997% pure powder, Showa Denko, Japan) and the assembly heated to the test temperature at 50°C/min. After the experiment, the assembly was furnace-cooled (cooling rate between ~130°C/min at 1000°C and ~30°C/min at the melting point of the tin alloy, 221°C). The contact angles and drop radius were measured using a program developed in our group.[5] Advancing drop experiments were performed starting from small cubes of metal (approximately 1 mm^3), while receding drop experiments were conducted using ~1 cm diameter disks of same volume (thickness around 20 μm).

In order to determine the operative transport mechanism at the metal-ceramic interface and the corresponding diffusivities or solution-precipitation rates, the time evolution of the interfacial grain boundary grooves was analyzed. After experiments at 1000°C, the metallic drop was dissolved using *aqua regia* (1/3 nitric acid, 2/3 hydrochloric acid) in order to observe the surface of the alumina substrate under the alloy. On these samples, the profiles of the grooves at the solid-liquid and solid-vapor interfaces were measured using AFM line analysis in the constant-force mode (Park Scientific Instruments M5), and the microstructure was observed using Scanning Electron Microscopy associated with Energy Dispersive X-Ray Spectroscopy (SEM-EDS, ISI-DS130C with an EDAX DX-4 spectroscope) and x-ray photoelectron spectroscopy (XPS, Physical Electronics PHI 5400 ESCA).

Cross-sectional transmission electron microscopy (TEM) samples were cut with a low-speed diamond disk to a thickness of 0.5 mm, then thinned with planar tripod polishing on diamond lapping disks to a thickness of 20 μm, and finally thinned to electron transparency by using a focused ion beam (FIB, FEI-Xpert, NCEM). They were observed by conventional TEM at 200 kV associated with EDS (JEOL 200CX with Kevex microanalysis), or high resolution energy filtered TEM (Phillips CM200 with Gatan Image Filter (GIF), and Link EDS detector).

RESULTS

Spreading kinetics

The melting point of the Sn-3 wt% Ag eutectic is 221°C. At temperatures below 550°C, a solid oxide layer encapsulates the liquid metal, impeding contact of the liquid with the alumina. Above 550°C, this layer disappears, leaving a shiny drop surface; the liquid then enters in contact with the substrate and spreading occurs. Thus, sessile-drop experiments were performed at temperatures between 600 and 1000°C. The wetting kinetics at 600°C is summarized in Fig. 1(a). The final contact angle is strongly influenced by the addition of titanium. Indeed, an addition of 1 wt% titanium into a Sn3Ag alloy can lead to a decrease of the final contact angle from 115° to 23°. It should also be pointed out that the final contact angles measured in receding drops can be larger than the lowest values measured for advancing fronts. Figure 1(b) shows that the drop diameter increases continuously until a stationary contact angle is reached. Image analysis show no measurable volume decrease of the metal drop after the stationary contact angle is reached, and the radius of the drop increases continuously during the experiment, indicating that the decrease of the contact angle is not due to the effect of evaporation combined with a pinned triple line, as has been observed in other systems.[6] Figure 1(c) shows the stationary contact angles measured after 60 minutes, at different temperatures. The variability is wide. A clear dependence of contact angle with temperature does not emerge. The lowest-measured (stationary) contact angles are independent of the temperature.

The variation of contact angles over time can be empirically described using an exponential decay function: $(\theta = \theta_f + (\theta_i - \theta_f)\exp\left(-\left(\dfrac{t}{\tau}\right)^n\right))$, where θ_i and θ_f are the initial and final contact angles, and τ is a characteristic spreading time that typically varies between 50 and 800 seconds (Fig. 2(a)) and n ranges between 0.5 and 1. The drop radius variations follow a parallel exponential increase (with n and τ in the same range). Our measured spreading velocities are several orders of magnitude lower than those typically measured for low

temperature liquids of similar viscosity and for metal-metal systems using a drop transfer set-up[7,8] (Fig. 2(b)), but of the order of those frequently reported for small braze drops in sessile drop experiments.[9]

Grain Boundary Grooving

The presence of titanium dramatically enhances atomic transport close to the metal–ceramic interface at 1000°C. Grain boundary grooves are clearly visible at the Sn3Ag1Ti/alumina interface, but can not be observed on the free alumina surfaces (Fig. 3(a)) or at the interface between alumina and Sn3Ag (without Ti). Figure 3(b) shows the typical microstructure of the alumina surface under the Sn3Ag1Ti drop. Small islands of Ti-rich reaction product (cone-shaped, ~1 μm in diameter) and facets on the alumina grains can be observed. The AFM profiles (Fig. 3(c)) show humps on each side of the groove, indicating that its evolution is controlled by interfacial or volume diffusion and not solution/precipitation.[10–13]

Microstructure

The starting alloy has a typical tin-silver eutectic microstructure that seems qualitatively the same after the wetting experiment: Sn_5Ti_6 platelets are dispersed in a matrix made of Ag_3Sn dendrites surrounded by pure tin (Fig. 4). No continuous reaction layer could be observed on the alumina surface, although after experiments at the higher temperatures some isolated islands of reaction products were observed. No significant variation in the size of the Sn_5Ti_6 platelets could be measured after the experiments.

At temperatures of 700°C and below, SEM and cross sectional TEM observations show no evidence of substrate dissolution. On some samples, after cooling a discontinuous reaction layer at the Sn/Al_2O_3 interface is detected by TEM (Figs. 5(a) and 5(b)). The layer consists of isolated islands, several microns wide and 5–75 nm thick, formed by Ti-rich nanoparticles. No reaction phases can be observed at the interface between Ag_3Sn grains and alumina.

Experiments at temperatures above 800°C have provided clear evidence of substrate dissolution. Large islands of reaction product (around 10 μm in diameter and 1 μm thick) are seen by optical microscopy and SEM (Fig. 5(c)). They are found mainly on surface

heterogeneities (such as scratches or triple-line ridges) and in the center of the drop (where the metal and ceramic have been in contact for a longer time). Numerous, small reaction islands around 1 μm wide are observed by SEM (Fig. 5(d)). Cross-sectional TEM observations systematically show the presence of these discontinuous reaction islands partly buried in the alumina (5-50 nm thick, and 200 nm to 1 μm wide), much smaller but more numerous than those observed after experiments at lower temperatures (Figs. 5(e) and 6). EDS analyses show that the interfacial reaction phase is formed by titanium and oxygen. XPS experiments suggest that it is a titanium oxide, either TiO_2 or Ti_2O_3 (Figure 5).[14-20] In spite of their variability due to stresses, the inter-reticular distances measured on the HRTEM picture shown on Fig. 6 make TiO_2 more probable.

A continuous reaction layer covering the interface is never observed at any temperature. In some cases (independent of the temperature) 15 to 30 nm high triple-line ridges can be seen on the alumina surface of drop-free specimens (Fig. 7). The ridge can act as a nucleation site for the creation of reaction products (Fig. 5(c)).

DISCUSSION

The equilibrium oxygen partial pressure $p(O_2)$ for the reaction $Sn+O_2 \rightarrow SnO_2$ ranges between ~10^{-50} Pa at 250°C to ~10^{-16} Pa at 1000°C.[21] Therefore, considering only the oxidation of tin, a tin oxide layer around the metallic drop should be always stable at the temperature range of our experiments. The strong affinity of titanium for oxygen also contributes to the formation of an oxide layer encapsulating the metal. The formation of resilient oxide layers on the surface of low-temperature-melting metals in vacuum is well documented.[22-26] Typically, there is a critical temperature at which the oxide layer disappears (for Sn-3%Ag-1%Ti in our furnace, it was measured around 550°C in vacuum); three reasons for this have been proposed: (1) erosion through formation of volatile species;[23–25] (2) cracking due to volume changes and thermal-expansion mismatch;[23,24,26] and (3) dissolution of the oxide in the metal.[22] Above the critical temperature at which the oxide layer disappears, the metal vapour should react with the oxygen in the atmosphere, leading to an oxygen activity around the drop

6

equal to or even lower than the equilibrium $p(O_2)$ for the oxidation of the metal.[26] The metallic drop surface is then free of surface oxide layers, and spreading can occur.

Spreading Kinetics

Most models of reactive spreading assume that the reaction product and the liquid front advance simultaneously.[27-29] The interfacial microstructures observed in our experiments contradict this assumption since no continuous reaction layer could ever be observed, indicating that the liquid and the reaction product did not advance simultaneously, and suggesting that the observed decrease in contact angle for the Sn3Ag1Ti alloy is driven by the adsorption of Ti-species prior to the nucleation of the reaction product. This situation can be more general than commonly believed since there is evidence of discontinuous reaction layers in several other reactive systems.[30,31]

The recorded spreading velocities are not consistent with fluid-flow or adsorption-controlled spreading[1]; in both cases, much faster spreading is expected. In the starting alloy there is an inhomogeneous distribution of Sn_5Ti_6 platelets that dissolve slowly in the molten metal, enriching the liquid in Ti. The spreading velocities can be controlled either by the kinetics of Ti dissolution into the liquid or the transport of Ti to the triple junction. Depending on the transport distance, Ti transport can be controlled either by diffusion (on small distances) or by the convection movements in the liquid.[32] Considering that the diffusion coefficient of Ti in the liquid is close to 10^{-9} m^2·s^{-1}, the diffusion speed of Ti in the drop is close to $4 \cdot 10^{-5}$ m·s^{-1}. This is larger than the maximum measured spreading velocity (Figure 3(b)). The transport by convection is even faster. Thus we can assume that spreading kinetics is not controlled by transport of titanium to the triple line but by the kinetics of Ti dissolution into the liquid.

Adsorption of Ti-species at the interface can decrease all the interfacial energies (γ_{sv}, γ_{sl}, and γ_{lv}). The microstructural analysis shows that the reaction product is not continuous, indicating that its nucleation is sufficiently slow for the liquid front to move on an unreacted substrate. The corresponding liquid-solid metastable interfaces will have well-defined properties, which

may include low interfacial energy owing to adsorption of Ti-species prior to reaction. The velocity of the liquid front is one order of magnitude slower than diffusion velocities and also much slower than the maximum critical velocity above which adsorption at the triple line can not accompany spreading and influence the driving force.[1] We can assume that, at a given time, the interfacial energies at the triple line are the metastable values that correspond to a liquid with a given Ti concentration on an unreacted surface. In the simplest approximation, this relationship can be described using Langmuir adsorption isotherms than can be prolonged into the metastable regime to describe the expected decrease in interfacial energy (Fig. 8). Then the instantaneous contact angle can be related to the Ti concentration through the corresponding interfacial energies using the following well-known equation:

$$\cos(\theta) = \frac{\gamma_{sv} - \gamma_{sl}}{\gamma_{lv}} \tag{1a}$$

or

$$\cos(\theta(a_{Ti})) = \frac{\gamma_{sv}(a_{Ti}) - \gamma_{sl}(a_{Ti})}{\gamma_{lv}(a_{Ti})} \tag{1b}$$

Let's assume that the adsorption of titanium only occurs on the solid-liquid interface. In the simplest approximation, the effect of Ti on the interfacial energy can be described using the Langmuir adsorption isotherm:[33]

$$\gamma_{sl}(t) = \gamma_{sl}^{0} - \gamma_{ad} \ln\left(1 + \frac{a_{Ti}(t)}{a_c}\right) \tag{2}$$

$$\gamma_{ad} = \frac{kT}{\sigma_0} \tag{3}$$

where γ_{sl}^{0} is the solid-liquid surface energy without adsorbates, $\gamma_{sl}(t)$ is the solid-liquid surface energy, σ_0 is the Ti coverage at the metal/alumina interface, $a_{Ti}(t)$ is the titanium activity (using an ideal solution approximation where the activity is equal to the Ti concentration $C_{Ti}(t)$) and a_c is a critical titanium activity that marks the Ti concentration above which adsorption will occur at the metal-ceramic interface. If γ_{lv}^{0} is the liquid-vapor surface energy and θ_0 the equilibrium contact angle of a Sn3Ag drop without titanium on sapphire, equation (1) becomes:

$$\cos(\theta(t)) = \frac{\gamma_{lv}^{0}\cos(\theta_0) - \gamma_{ad}\ln\left(1 + \dfrac{C_{Ti}(t)}{a_c}\right)}{\gamma_{lv}^{0}} \qquad (4)$$

A rough calculation of the Ti dissolution kinetics can be made, taking into account the repartition of titanium inside the tin alloy. To simplify, we will consider that for a given time, t, the liquid metal contains N Sn_5Ti_6 spheres of radius $R(t)$ per unit of volume. Assuming that the number of Ti atoms leaving the particles per unit of time is proportional to $(C(t) - C_s))$ (where $C(t)$ is the Ti concentration in the liquid at the time t, and C_s is the Ti saturation concentration in tin) and is also proportional to the total surface of the particles, it is possible to calculate the radius of the particles and thus the titanium concentration in the liquid metal versus time. Thus, replacing $C_{Ti}(t)$ by its calculated value allows the calculation of the curves shown in Figure 2. In this calculation, we assume that σ_0 corresponds to one adsorbed monolayer; that the critical activity a_c of Ti is between 0.03% and 0.1%;[1] that the initial dissolution rate of the platelets is between 1 and $5\cdot10^{-6}$ cm·s^{-1}; and that θ_0 is 105 degrees (the lowest-measured value for pure tin on sapphire[22]). All these approximate values are in agreement with literature[1] and our experiments.

Even with the simplifying assumptions (adsorption of one monolalyer of Ti only at the solid/liquid interface) and rough estimates of some of the parameters (in particular the dissolution rates of the Sn_5Ti_6) the predicted spreading times are of the order of those

recorded. A more accurate model will have to be developed to verify these assumptions more carefully.

The experiments show a large degree of variability in the final contact angles. There are two possible and complementary explanations: occasional ridge formation at the triple line that can pin the drop front, and variability in the dissolution of the Sn_5Ti_6 platelets. It has been proposed that in high temperature systems the formation of triple line ridges can be the source of large wetting hysteresis.[1] Triple-line ridges can form by local diffusion or solution-precipitation in order to achieve full two-dimensional equilibrium of the interfacial forces at the triple junction. If the liquid front remains attached to the ridge, the spreading kinetics will be controlled by the ridge movement (Regime II or Regime III spreading).[6] Ridge evolution depends on the diffusion or solution-precipitation rates, and ridge-controlled spreading is expected to be orders of magnitude slower than fluid flow or adsorption controlled wetting. Our results indicate that in some cases, ridges can nucleate at the triple line. The observed ridges are usually smaller than 20 nm. Above 800°C, the ridge can act also as a nucleation site for the formation of reaction product. The ridge angle is very wide (more than 170 degrees, as measured by AFM in Fig. 7).

Provided that the diffusion at the solid-vapor interface is negligible compared to the diffusion at the solid-liquid interface ($D_{sv} << D_{sl}$), the steady state speed (which is also the maximum speed) of an advancing ridge moving through interfacial diffusion is given by equation (5a).[34] If $D_{sv} \approx D_{sl}$ then equation (5b) should apply.[10,34]

$$v_{ss}^{Adv} = \frac{\omega D_{sv} \gamma_{sv} \Omega}{kT} \left(\frac{\tan(\pi - \phi_s)}{h} \right)^3 \tag{5a}$$

$$v_{ss}^{Adv} = \frac{\omega D_{sv} \gamma_{sv} \Omega}{kT} \left(\frac{\tan(\pi - \phi_s)}{3h} \right)^3 \tag{5b}$$

Where ϕ_s is the angle of the ridge (~170 deg measured by AFM), and h its height. ωD_{sv} is the interfacial diffusivity at the solid-vapor interface (~10^{-27} $m^3 \cdot s^{-1}$ at 1000°C, extrapolated from Dynys et al.[35]) and γ_{sv} is the surface tension of alumina (~1.6 $J \cdot m^{-2}$ at 1000°C[36]).

Using equations (5a) or (5b), the speed of a 20 nm high advancing ridge should be around 10^{-15} m·s^{-1}. This is much slower than the measured spreading rates at the same temperature (Fig. 2(b)). The recorded spreading velocities correspond to a ridge much smaller than 1 nm. In the range of temperatures used in this work, spreading kinetics is not controlled by ridge movement but rather by the dissolution kinetics of Ti in the molten alloy. However ridge formation can be initiated by defects on the alumina surface and will depend on the amount of Ti in the liquid since this amount affects the interfacial transport rates. According to equations (5a) and (5b), a ridge taller than 1 nm will move less than 1 μm during the experiment, thus pinning the triple line and effectively stopping spreading. Consequently, the observed ridges could account for the large variability of the final contact angles.

The slow pumping of Ti from the Sn_5Ti_6 platelets can also result in an increased variability, the activity of titanium being then very sensitive to the microstructure of the drop, which is not easily controlled. This variability also accounts for the relatively wide range of values calculated for τ, in particular at lower temperature where dissolution is expected to be slower.

Grain Boundary Grooving

The grain boundary groove profiles at the $Sn3Ag1Ti/Al_2O_3$ interface (Figure 4c) exhibit humps on either side of the roots, indicating that, in the time range investigated here, their growth is limited by diffusion, rather than the dissolution/precipitation rates. However, transport of the Al_2O_3 involves diffusion of both Al and O ions. This could occur either through the liquid metal, along the interfaces, or through the oxide itself. Volume diffusion through the Al_2O_3 is probably not important, based on rough calculations (the diffusion coefficients of Al and O in alumina are lower than 10^{-18} cm^2·s^{-1} at 1000°C, more than 10 orders of magnitude lower than in liquid metals[37]). Although each species could move independently along either path, the dissolution and deposition must involve stoichiometric Al_2O_3, setting a requirement that the sum of the departure and arrival rates from both paths balance locally. The transport of the slowest species through the fastest path will control

groove evolution. If interfacial diffusion is the fastest path, the time evolution of the groove width, w, can be approximated as:

$$w = 4.6(B_i t)^{1/4} \qquad (6)$$

Where B_i is the interfacial transport coefficients of the slowest species (at the solid-liquid interface):

$$B_i = \frac{\omega D_i \gamma_i \Omega}{kT} \qquad (7)$$

The corresponding interfacial diffusivities (10^{-20} $m^3 \cdot s^{-1}$) for the Sn3Ag1Ti system would be much larger than any surface diffusivity ever reported, even for the most impure aluminas ($\sim 10^{-27}$ $m^3 \cdot s^{-1}$).[35] It is then logical to assume that groove evolution is controlled by volume transport through the liquid, as has already been observed in other metal/alumina systems.[34] For a groove growth controlled by volume diffusion:

$$w = 5(B_v t)^{1/3} \qquad (8)$$

B_v is the corresponding volume transport coefficient:

$$B_v = \frac{x D_v \gamma_i \Omega}{kT} \qquad (9)$$

where x is the solubility of the controlling species and D_v the volume diffusion coefficient. Assuming that γ_i is γ_{sl} (~ 1.1 $J \cdot m^{-2}$ calculated from Nikolopoulos[38]) and that $\Omega/2$ is $\sim 2 \cdot 10^{-29}$ m^3 (volume per diffusing ion), the approximate volume diffusivities and corresponding solubility can be calculated (Table I). The large diffusivities measured in the SnAgTi/Al$_2$O$_3$ system are consistent with the lower oxygen activities expected in the presence of Sn$_5$Ti$_6$ platelets and

the reports of enhanced transport at liquid metal/alumina interfaces at very low oxygen activities.[34]

The evolution of the grain boundary grooves will be controlled by the species with lowest diffusivity (xD_V). Because diffusion coefficients through liquid metals are very similar for different species, grooving will be controlled by the species with lower solubility. Due to the presence of the dispersed Sn_5Ti_6 platelets, the activity of oxygen in the liquid is expected to be very low; consequently, grooving is expected to be controlled by the transport of the oxygen-rich species. Considering that D_v is close to 10^{-9} $m^2 \cdot s^{-1}$, a typical value for liquid metals,[39] the estimated solubility of the slow species is ~10^{-5}. This large oxygen activity emphasizes the fact that the liquid Sn-Al-O does not form an ideal, which has also been observed for other metal-alumina systems.[40] It has also been proposed that at very low oxygen activities, transport through both paths (volume and interface) can contribute to the evolution of the grooves, resulting in accelerated grooving rates.[34]

Microstructure

The experiments clearly show that the addition of Ti enhances the wetting of Sn3Ag alloys. It has often been proposed that the effect of the reactive elements (such as Ti, Cr, and others) on the wetting behavior of liquid alloys on ceramics is related to the formation of interfacial reaction layers.[31] Our results also indicate that the addition or a reactive element improves wetting even though no continuous reaction layer could be observed at any temperature. There is a finite barrier for the nucleation of the reaction phase, and the reaction product and the liquid do not extend together. This is confirmed by Fig. 5(c), which shows a clearly discontinuous reaction product. One difference between this system and other brazing alloys is that the dissolution of Ti into the liquid seems to occur at much slower rate (the size of the Sn_5Ti_6 platelets of the starting alloy and of the drop after cooling are similar). The slower pumping rate of Ti into the liquid helps to better differentiate between the effects of adsorption and reaction. Comparison of the HRTEM, EDS and XPS analyses with published data[14-19] at the interface between Al_2O_3 and Ti-containing brazing alloys suggests that the reaction phase is a Ti oxide.[1] It is not clear whether the reaction product is TiO_2 or Ti_2O_3,

although HRTEM and EDS-TEM analyses show that a distorted TiO_2 is more probable, and it forms either at high temperature or during cooling. As the oxygen activities in the system are not measurable, no thermodynamical consideration can help distinguish between these two oxides. Figure 5(e) shows TEM micrographs of a SnAgTi/sapphire interface after a wetting experiment at 1000°C. The Ti oxide islands are partially buried in the alumina surface suggesting that they grown concurrently with alumina on the sapphire substrate, probably from to precipitation during cooling of dissolved Ti and Al oxide.

We can summarize the formation of the microstructure at the interface as follows:

1- During heating and at high temperature, partial dissolution of the Sn_5Ti_6 platelets occurs.

2- The substrate is dissolved locally, leading to the Al enrichment of the metal and to the creation of surface defects.

3 Ti oxides nucleate on defects at the interface. The reaction product is more abundant in the centre of the drop where the metal has been in contact with the sapphire for a longer time.

4 Al and Ti oxides precipitate further during cooling.

CONCLUSION

Small Ti additions can decrease the contact angle of Sn3Ag on alumina from 115° to 23°, allowing the use of Sn3Ag-based lead-free solder to bond alumina at low temperature. The spreading kinetics are not compatible with any model developed for low temperature spreading. Our results underline the fact that a comprehensive analysis of reactive spreading should divide the process into its constituent steps (fluid flow, adsorption of reactive element, nucleation of the reaction product, and probably ridging) and determine their relative kinetics. In that way, the structure and composition of the triple junction for each stage can be analyzed in order to identify which step drives the decrease of contact angle as well as which process controls the spreading kinetics for a given system. In the case of Sn3Ag1Ti alloys spreading

on alumina, the spreading kinetics is controlled by the speed of dissolution of Ti into the liquid, but the addition of Ti enhances the atomic transport at the metal-ceramic interface, resulting in the formation of triple-line ridges that pin the liquid front and result in a wide variability of the final contact angles. The results are consistent with the hypothesis that adsorption of Ti species previous to a reaction decreases the solid-liquid interfacial energy and promotes wetting. This scenario may be more typical than what is usually believed.

REFERENCES

1. E.Saiz, R.M. Cannon and A.P. Tomsia: Reactive spreading: adsorption, ridging and compound formation. Acta Mater. 48, 4449 (2000).

2. M. Abtew and M. Selvaduray: Lead-free solders in microelectronics. Mater. Sci. Eng. R 27, 95 (2000).

3. E. Saiz, C.H. Hwang, K. Suganuma and A.P. Tomsia: Spreading of Sn-Ag solders on FeNi alloys. Acta Mater. 51, 3185 (2003).

4. B. Derby and J.R.P. Webster: Neutron Reflection Study of the composition of interfaces between titanium-containing active braze alloys and sapphire. Transactions of the Japanese Welding Research Institute 30, 233 (2001).

5. L. Gremillard, *DropAngle*, software, LBNL, (2004), available upon request to the author.

6. E. Saiz, A.P. Tomsia and R.M. Cannon: Ridging effects on wetting and spreading of liquids on solids. Acta Mater. 46, 2349 (1998).

7. S.F. Kistler: Hydrodynamics of wetting. In Wettability, edited by J.C. Berg (New York: Marcel Dekker Inc, 1993).

8. E. Saiz, A.P. Tomsia: Atomic dynamics and Marangoni films during liquid-metal spreading. Nature Materials 3, 903 (2004).

9. N. Eustathopoulos, A. Koltsov, M. Dumont, F. Hodaj: Influence of Ti on wetting of AlN by Ni-base alloys. Mater. Sci. Eng. A415, 171 (2006).

10. W.W. Mullins: The effect of thermal grooving on grain boundary motion. Acta Met. 6, 414 (1958).

11. W.W. Mullins: Grain Boundary grooving by volume diffusion. Trans. Metall. Soc. A.I.M.E. 218, 354 (1960).

12. W.W. Mullins: Theory of thermal grooving. J. Appl. Phys. 28, 333 (1957).

13. W.W. Mullins, and Shewmon PG: The kinetics of grain boundary grooving in copper. Acta Met. 7, 163 (1959).

14. J.F. Moulder, W.F. Stickle, P.E. Sobol, K.D. Bomben. In: Handbook of X-ray photoelectron spectroscopy, edited by J. Chastain and R.C. King Jr. (Physical Electronics, MN USA, 1995).

15. W.S. Oh, C. Xu, D.Y. Kim and D.W. Goodman: Preparation and characterization of epitaxial titanium oxide films on Mo(100). J. Vac. Sci. Technol. A15, 1710 (1997).

16. K. Baba and R. Hatada: Preparation and properties of nitrogen and titanium oxide incorporated diamond-like carbon films by plasma source ion implantation. Surf. Coatings Technol. 136, 192 (2001).

17. H.K. Jang, S.W. Whangbo, Y.K. Choi, Y.D. Chung, K. Jeong, C.N. Whang, Y.S. Lee, H.S. Lee, J.S. Choi, G.H. Kim, and T.K. Kim: Titanium oxide films on Si(100) deposited by e-beam evaporation. J. Vac. Sci. Technol. A 18, 2932 (2000).

18. F. Zhang, G.K. Wolf, X. Wang and X. Liu: Surface properties of silver doped titanium oxide films. Surf. Coatings Technol. 148, 65 (2001).

19. Y. Gao, Y. Liang and S.A. Chambers: Thermal stability and the role of oxygen vacancy defects in strong metal support interaction - Pt on Nb-doped TiO_2(100). Surf. Sci. 365, 638 (1996).

20. B. Feng, J. Weng, B.C. Yang, J.Y. Chen, J.Z. Zhao, L. He, S.K. Qi and X.D. Zhang: Surface characterization of titanium and adsorption of bovine serum albumin. Materials Characterization 49, 129 (2003).

21. J.A. Dean: Lange's handbook of chemistry 14th ed. (McGraw-Hill, New York, USA, 1992), pp. 6.88 – 6.129.

22. I. Rivolet, D. Chatain and N. Eustathopoulos: Wettability of alumina single crystals with gold and tin between their melting point and 1673 K. Acta Met. 35, 835 (1987).

23. V. Laurent, D. Chatain, C. Chatillon and N. Eustathopoulos: Wettability of monocrystalline alumina by aluminium between its melting point and 1273 K. Acta Met. 36, 1797 (1988).

24. J.J. Brennan and J.A. Pask: Effect of the nature of surfaces on wetting of sapphire by liquid aluminum. J. Am. Ceram. Soc. 51, 569 (1968).

25. E. Ricci and A. Passerone: Review – Surface-tension and its relations with adsorption, vapourization and surface reactivity of liquid-metals. Mater. Sci. Eng. A161, 31 (1993).

26. W. Jung, H. Song, S.W. Park and D. Kim: Variation of contact angles with temperature and time in the Al-Al2O3 system. Met. Mat. Trans. B27, 51 (1996).

27. N. Eustathopoulos and B. Drevet: Interfacial bonding, wettability and reactivity in metal/oxide systems. J. Phys. III 4, 1865 (1994).

28. I.A. Aksay, C.E. Hoge and J.A. Pask: Wetting under chemical equilibrium and non-equilibrium conditions. J. Phys. Chem. 78, 1178 (1974).

29. F.G. Yost and A.D. Romig Jr: Thermodynamics of wetting by liquid metals, in Electronic Packaging Materials Science II, edited by R.C. Sundahl, R. Jaccodine, and K.A. Jackson (Mater. Res. Soc. Symp. Proc. 108, 1988), p. 385.

30. R. Loehman, F.M. Hosking, B. Gauntt, P.G. Kotula, P. Lu: Reactions of Hf-Ag and Zr-Ag alloys with Al2O3 at elevated temperatures. J. Mater. Sci. 9-10, 2319 (2005).

31. A. Meier, P.R. Chidambaram and G.R. Edwards: Modelling of the spreading kinetics of reactive brazing alloys on ceramic substrates: Copper-titanium alloys on polycrystalline alumina. Acta Mat. 46, 4453 (1998).

32. A. Mortensen, B. Drevet, N. Eustathopoulos: Kinetics of diffusion-limited spreading of sessile drops in reactive wetting. Scripta Mat. 36 645 (1997).

33. A.W. Adamson: Physical chemistry of surfaces (Interscience Publishers, New York, NY, 1963).

34. E. Saiz, R.M. Cannon and A.P. Tomsia: Energetics and atomic transport at liquid metal/Al2O3 interfaces. Acta Mater. 47, 4209 (1999).

35. J. Dynys, R.L. Coble, W.S. Coblenz and R.M. Cannon: Mechanisms of atom transport during initial stage sintering of Al_2O_3, in Sintering Processes, edited by G.C. Kuczynski, (Plenum Press, New York, NY, 1980) p. 391.

36. O. Kubachevsky and C.B. Alcock: Metallurgical Thermochemistry, 1st Ed. (Pergammon Press, New York, NY, 1979), pp. 388-390.

37. N. Louet, Influence of calcia and silica doping on sintering and microstructural evolution of ultrapure alpha-alumina (in French), PhD Thesis, INSA Lyon, France, 2003.

38. P. Nikolopoulos: Surface, Grain-boundary and interfacial energies in Al_2O_3 and Al_2O_3-Sn, Al_2O_3-Co systems. J. Mater. Sci. 20, 3993 (1985).

39. C.J. Smithells (ed.): Metals Reference Book (Butterworths, London, England, 1976), p. 939.

40. K. Yoshihara and K. Nii: Effect of oxygen potential on surface self-diffusion coefficient of silver. J. Jap. Inst. Met. 42, 492 (1978).

System	Temp. (K)	$x.D_v$ ($m^2.s^{-1}$)	x
SnAgTi/Al$_2$O$_3$	1273	$1.7\ 10^{-14}$	$1.7\ 10^{-5}$
Al/Al$_2$O$_3$ [34]	1373	$5\ 10^{-14}$	$5\ 10^{-5}$
Ni/Al$_2$O$_3$ [34]	1773	$1.1\ 10^{-13}$	$1.1\ 10^{-4}$
Cu/Al$_2$O$_3$ [34]	1423	$3.5\ 10^{-18}$	$3.5\ 10^{-9}$
Au/Al$_2$O$_3$ [34]	1373	$7.8\ 10^{-16}$	$7.8\ 10^{-7}$

Table I: Calculated volume diffusivities. The solubility, x, is calculated assuming a volume diffusion coefficient inside the liquid metal of ~10-9 m2.s-1.

FIGURE CAPTIONS:

Figure 1: (a) Wetting kinetics for selected experiments performed at 600°C. ▲: advancing Sn3Ag drop. O: receding Sn3Ag1Ti drop. ■: advancing Sn3Ag1Ti drop. □: advancing Sn3Ag1Ti drop pinned by triple line ridging, thus reaching higher stationary contact angle.
(b) Diameter of the Sn3Ag1Ti advancing drop (■) shown on Figure 1(a) versus time; the continuous increase of the diameter indicates that the decrease of contact angle is due to spreading, and not to evaporation of the drop coupled with a pinned triple line.
(c) Evolution of final contact angle with temperature in the system Sn3Ag1Ti/Sapphire (advancing drop setup); note the wide variability of the results, especially at lower temperature.

Figure 2: (a) Evolution of the time constant τ (a measure of the spreading time required to reach a stationary contact angle) versus experimental temperature. The variability in the concentration of Sn_5Ti_6 platelets will result in variability in the kinetics of Ti enrichment in the liquid and can justify the observed wide range of calculated τ, in particular at lower temperature where dissolution of Ti is slower. (b) Plot of the contact angle vs. spreading velocity values. The velocities reached in our system can be 10^5 times lower than the velocities ruled by fluid flow. The continuous black lines indicate the speeds calculated after the Ti dissolution model, calculated for 25μm-sized Sn5Ti6 particles, θ_0 of 105 deg., σ_0 corresponding to 1 adsorbed monolayer, and with critical titanium activity and dissolution rates of the platelets of (1): 0.1mol% and 10^{-6} cm/s; (2): 0.06% and $3\ 10^{-6}$; (3): 0.04% and $4\ 10^{-6}$; (4): 0.03% and $5\ 10^{-6}$. The gray bands indicate typical maximum spreading velocities expected with other models.

Figure 3: (a) Optical microscope view of the limit between the drop-free surface and the metal-ceramic interface. (b) AFM view of a typical microstructure at the metal-alumina interface. (c) Typical AFM depth profiles across grain boundary grooves after 5 h at 1000°C. (d) Time evolution of the groove width (w), fitted with power laws: $w\ \alpha\ t^{1/3}$ corresponds to volume diffusion controlled grooving, whereas $w\ \alpha\ t^{1/4}$ corresponds to surface diffusion control.

Figure 4: Microstructure of the tin alloy after wetting experiment, showing Sn_5Ti_6 platelets (top) and Ag_3Sn dendrites (bottom) embedded in pure tin.

Figure 5: (a) and (b): Conventional-TEM observation of the interface between sapphire and Sn-3Ag-1Ti after 2 experiments at 600°C; (a) shows a discontinuous reaction layer; the EDS analyses (not shown) indicate a strong Ti enrichment on this layer. (c) Optical microscope view of the interface after an experiment at 900°C, showing islands of Ti-rich reaction products on the surface below the drop and the nucleation of reaction product along the triple line. (d) SEM view of the interface after an experiment at 1000°C, showing small islands of reaction product (1 μm wide) surrounding a bigger one (upper-right-hand corner). (e) C-TEM observation of the interface after a wetting experiment at 1000°C. Discontinuous islands of titanium oxide can be seen.

Figure 6: HR-TEM picture of the Sn3Ag1Ti/Sapphire interface, showing a layer of titanium oxide between the metal and the alumina. The inter-reticular distances are compatible with TiO_2.

Figure 7: Atomic Force Microscopy image of the ridge at the triple line on a polycrystalline alumina, after a wetting experiment at 1000°C. The depth profile along the white line shows an 18 nm high ridge.

Figure 8: Schematic showing a possible sequence for the wetting of Sn3Ag1Ti on alumina, as Ti from the Sn5Ti6 platelets dissolves, it adsorbs at the solid-liquid interface decreasing the interfacial energy and promoting spreading. If there is a finite nucleation barrier for the formation of the reaction product, extension of the adsorption isotherm into the metastable regime will result in a further decrease of the interfacial energy, even if some isolated islands of reaction product form at high temperature during spreading.
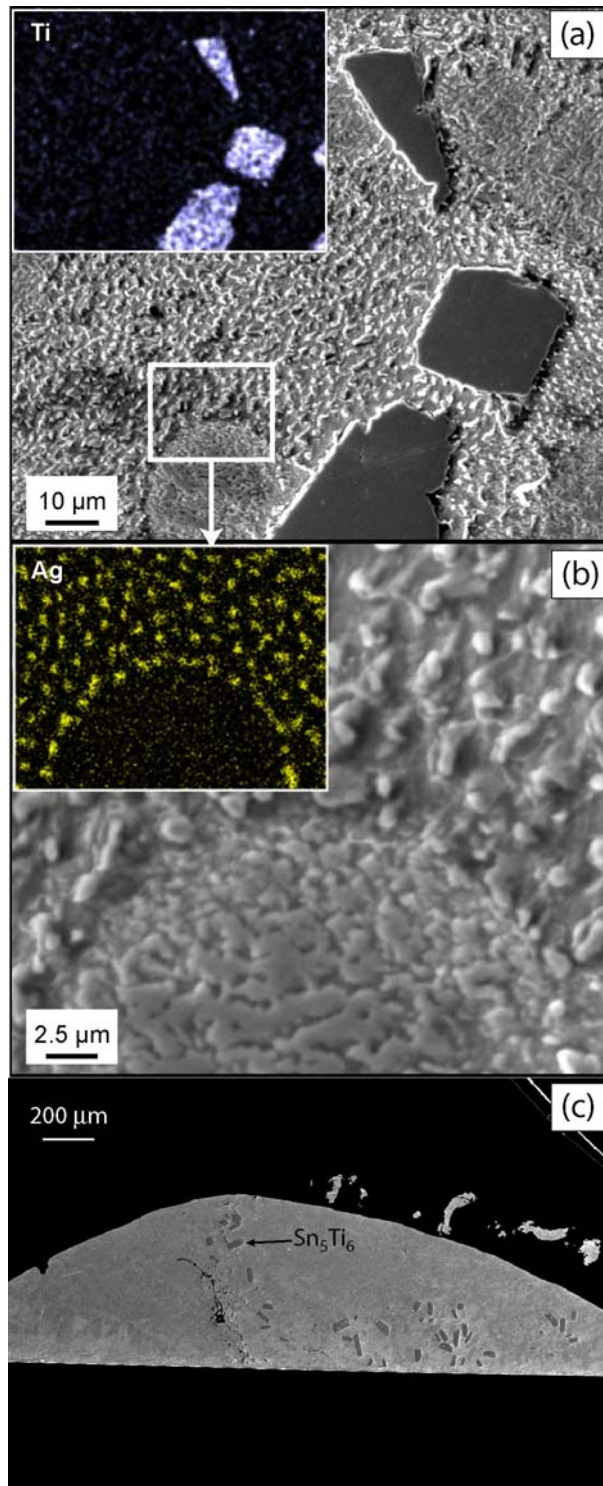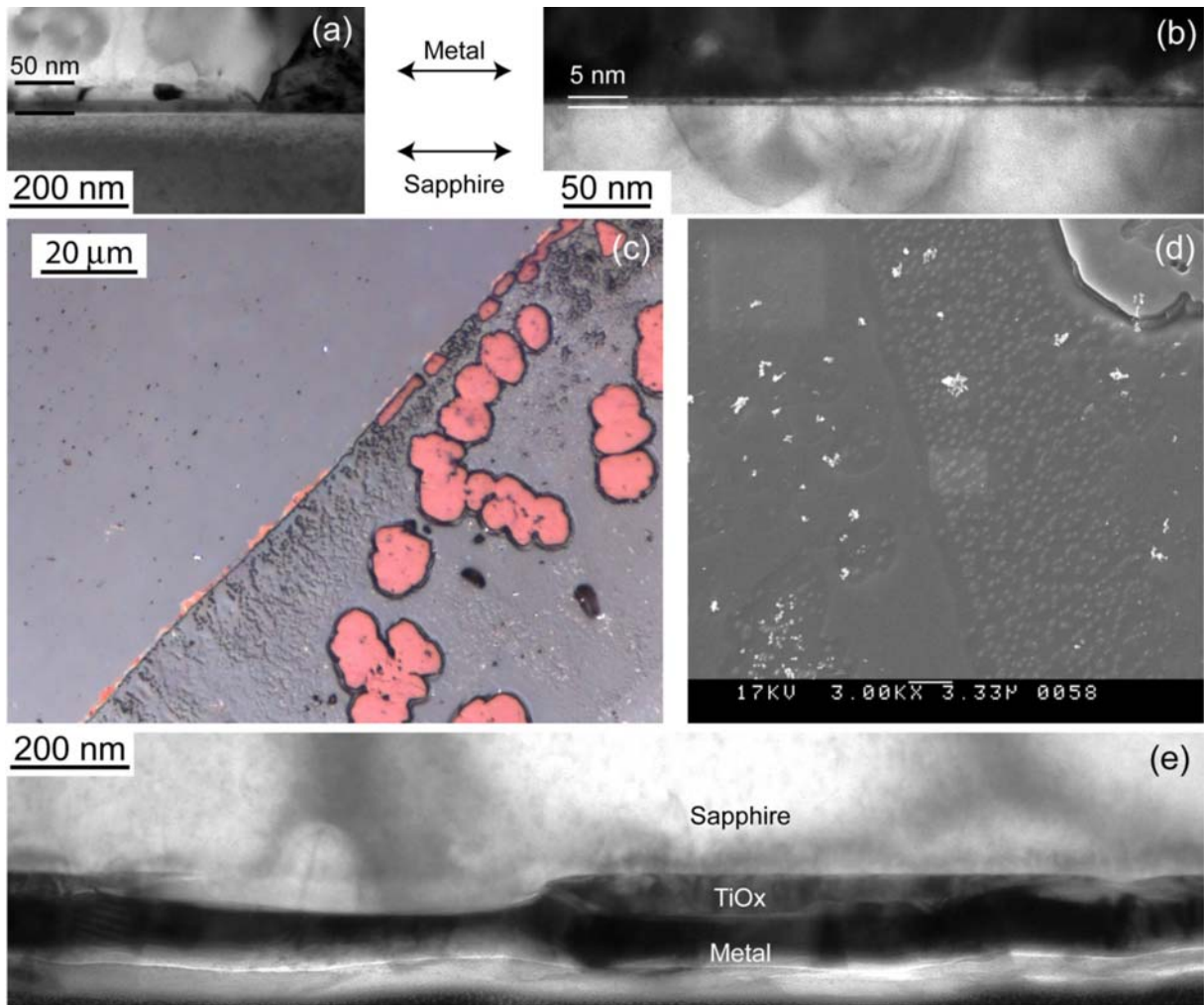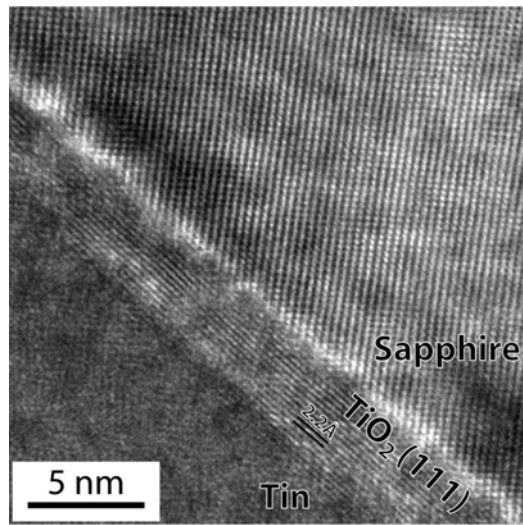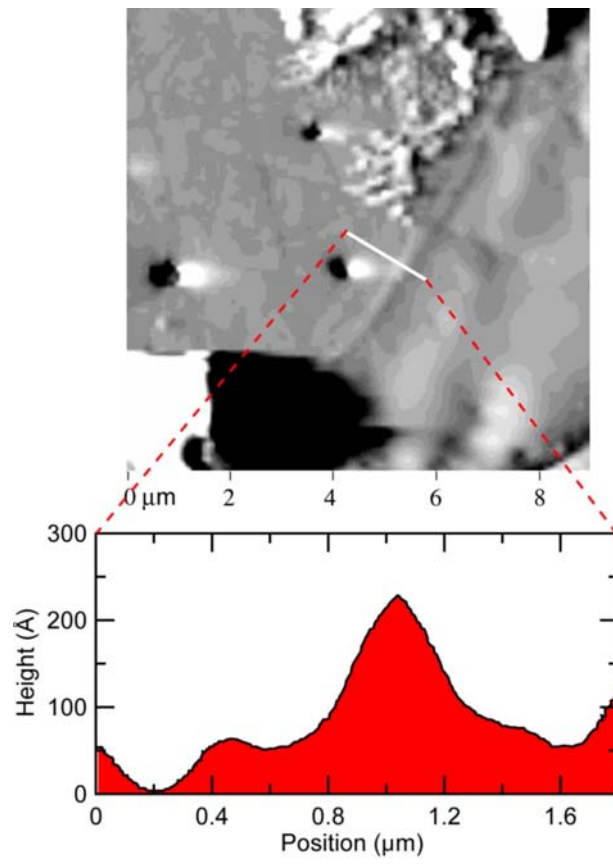
Figure 1
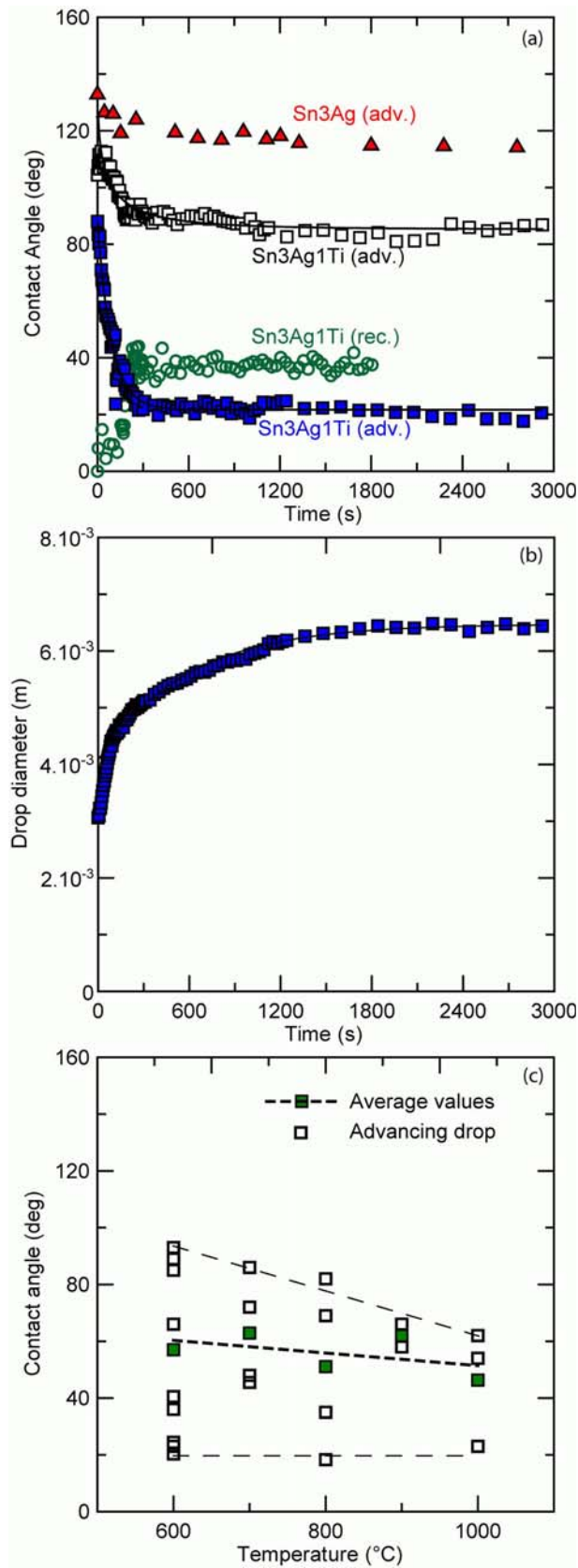
Figure 2
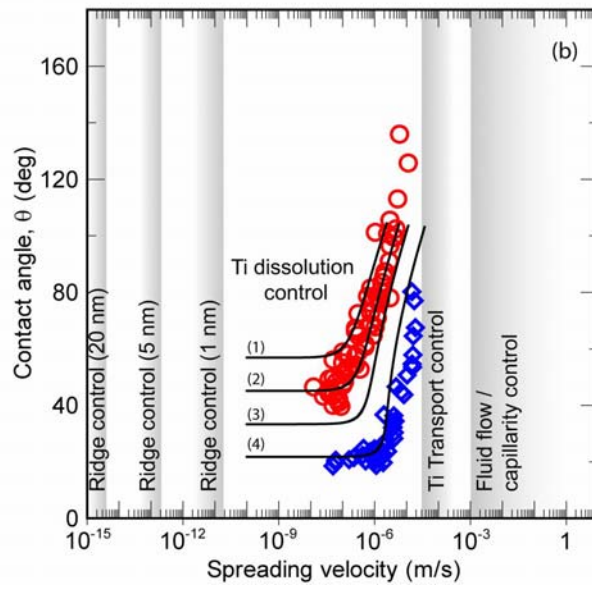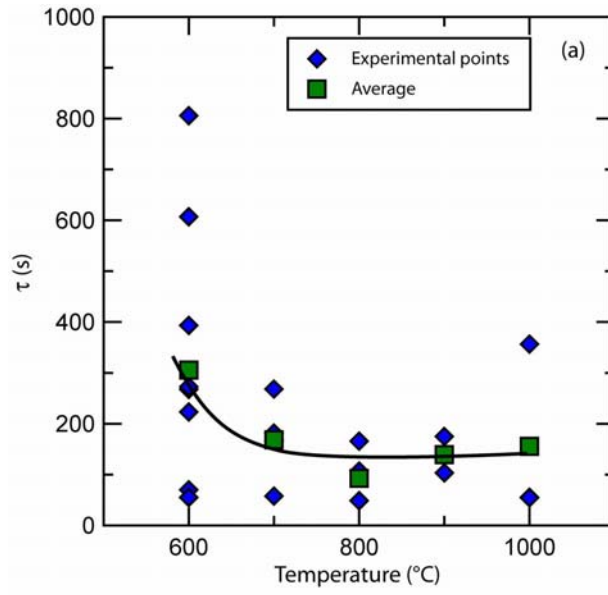
Figure 3
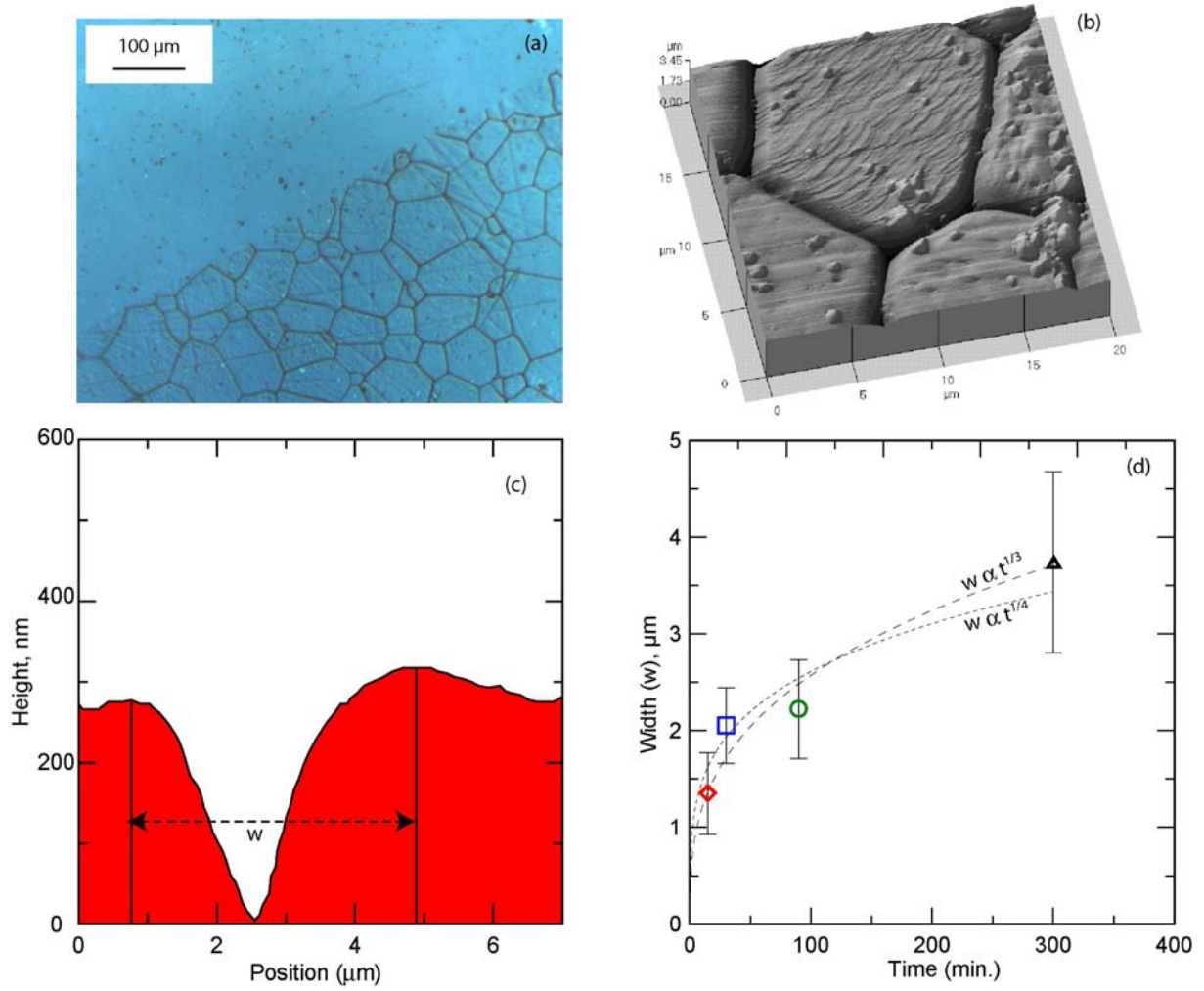
Figure 4

Figure 5

Figure 6

Figure 7

Figure 8